Ceramics International 45 (2019) 23399–23405

Contents lists available at ScienceDirect

Ceramics International

journal homepage: www.elsevier.com/locate/ceramint

Perovskite/polyethylene oxide composites: Toward perovskite solar cells without anti-solvent treatment

Seojun Lee[a], Jung Sang Cho[b,**], Dong-Won Kang[a,*]

[a] School of Energy Systems Engineering, Chung-Ang University, Seoul, 06974, Republic of Korea
[b] Department of Engineering Chemistry, Chungbuk National University, 28644, Republic of Korea

ARTICLE INFO

Keywords:
Polyethylene oxide
Perovskites
Anti-solvent
Morphology
Solar cells

ABSTRACT

In this study, polyethylene oxide (PEO) is introduced into methylammonium lead iodide ($MAPbI_3$) perovskite to replace the standard anti-solvent washing process of perovskite solar cells. By forming PEO-$MAPbI_3$ composites, we achieved controllability of the perovskite surface morphology. Furthermore, the PEO addition improved the electronic properties of the composites by suppressing the trap density of the $MAPbI_3$ perovskite. We observed a significant increase in the average power conversion efficiency (PCE) of the perovskite solar cells (PVSCs) from 0.24% to 7.25% using the proper PEO-perovskite composition ratio (1.5:1), based on their fabrication without any organic anti-solvent treatment. Moreover, the performance uniformity and outdoor stability were significantly enhanced by employing the composite. The proposed PEO-perovskite composite offers a promising pathway for the industrialization of PVSCs in terms of PCE, uniformity, stability, and feasibility—without involving current anti-solvent washing process.

1. Introduction

In recent years, perovskite solar cells (PVSCs) have received significant attention from researchers worldwide for their remarkable efficiency increase of nearly 24% compared to that of commercial Si solar cells [1–7]. Many studies have been conducted with the aim of commercializing PVSCs because of their advantages, such as a simple, low temperature solution process and inexpensive materials [8–12]. However, scalability remains a major obstacle in the commercialization of PVSCs. Thus far, the perovskite absorber layers of most lab-scale high-efficiency PVSCs have been made through an anti-solvent washing method that has many benefits, such as forming homogeneous and crystalline perovskite thin films readily and providing morphology control [13–17]. However, this anti-solvent washing process is more likely to cause difficulties in guaranteeing the uniformity of a thin film coated over a large area. Furthermore, there are human and environmental issues involved with the hazardous organic anti-solvents—such as chlorobenzene and toluene—used in several studies that have reported excellent efficiency using spin coating and anti-solvent washing [18–21]. Therefore, the development of a separate technology for controlling the morphology and crystal growth of perovskite without anti-solvent treatment could be important for commercialization.

Different from PVSCs, there have been several reports on perovskite light-emitting diodes (LEDs) that use perovskite layers produced without a washing process. One of these methods is to add an ionic insulating polymer—polyethylene oxide (PEO)—to the perovskite composite [22–26]. PEO has primarily been studied in LEDs because its addition to perovskite composites reduces the grain size; produces a uniform, pinhole-free perovskite layer; and increases electroluminescence—all of which are suitable for improving LED properties [22,26]. In planar PVSCs, several studies have focused on the charge transport layer, as well as a passivation layer, to improve the performance of the cells by enhancing the interface engineering and increasing the conductivity [17,27,28]. However, there have been few reports on the development of PEO-perovskite composites, and solar cells that use PEO as a light absorbing layer.

In this paper, we first report on the effect of improving the planar perovskite absorber layer properties and solar cell characteristics by adding PEO to a perovskite composite. For this, we performed structural, optical, and morphological analyses, and photovoltaic characterization according to the amount of PEO in each PEO-$MAPbI_3$ perovskite composite. It was found that the addition of PEO resulted in smaller grain size and morphology control. Additionally, steady-state photoluminescence (PL) measurements showed that PL was improved and trap-assisted recombination was suppressed. These results led to the improved open circuit voltage and increased power conversion

* Corresponding author.
** Corresponding author.
E-mail addresses: jscho@cbnu.ac.kr (J.S. Cho), kangdwn@cau.ac.kr (D.-W. Kang).

https://doi.org/10.1016/j.ceramint.2019.08.042
Received 1 July 2019; Received in revised form 24 July 2019; Accepted 5 August 2019
Available online 05 August 2019

Abbreviations

PVSC	perovskite solar cell
LED	light emitting diode
PL	photoluminescence
PCE	power conversion efficiency
ETL	electron transport layer
HTL	hole transport layer
XRD	X-ray diffraction
FE-SEM	field emission scanning electron microscopy
AFM	atomic force microscopy
UV–Vis	ultraviolet–visible
FWHM	full width at half maximum

efficiency (PCE) of the overall PVSC with exceptional stability. By this method, the photovoltaic characteristics can be improved without an anti-solvent washing process, which has been regarded as essential in the research and development of PVSCs. We expect this method will be widely applied as a base technology for the commercialization of PVSCs.

2. Materials and methods

2.1. Materials

Methylammonium iodide (MAI, Greatcell Solar Ltd), lead iodide (PbI_2, 99.9985%, Alfa Aesar), and polyethylene oxide (M.W. 100 000, Alfa Aesar) were used as precursors for the PEO-perovskites with dimethylformamide (DMF, 99.5%, Samchun Chemical) and dimethyl sulfoxide (DMSO, 99.8%, Samchun Chemical) used as solvents. For the NiO_x hole transport layer, nickel nitrate hexahydrate ($Ni(NO_3)_2{\cdot}6H_2O$, 99.999%), ethylene glycol (99.5%, Junsei), and ethylenediamine (EDA, 99.0%, Samchun Chemical) were used unaltered. To prepare the electron transport layer (ETL), phenyl-C61-butyric acid methyl ester (PCBM, 99.5%, Nano-C) was used with chlorobenzene (CBZ, mono, > 99.5%, Kanto Chemical) as a solvent.

2.2. Precursor preparation for PEO-perovskite films

To prepare the PEO-perovskite precursor solutions, a $MAPbI_3$ perovskite solution (MAI:PbI_2:DMSO = 1:1:1; 1.8 M in DMF) was stirred overnight and mixed with a PEO solution (16 mg mL^{-1} in DMF) according to the following v/v% ratios: no PEO, 1:1, 1.25:1, and 1.5:1. The PEO-perovskite solutions were then stirred for 30 min at 70 °C before spin-coating. The PEO-perovskite layer was spin-coated onto the NiO_x hole-transport layer (HTL) at 4000 rpm for 50 s, followed by annealing on a hot plate at 100 °C for 10 min. Regarding NiO_x precursor solution, it was made by dissolving 1 M nickel nitrate hexahydrate (0.291 g) with ethylenediamine (67 μL) in ethylene glycol of 1 mL. The solutions were stirred at room temperature during overnight.

Device Fabrication: ITO-coated glass substrates were cleaned sequentially with detergents, acetone, isopropanol, and deionized water by sonification (10 min for each step). After drying in an oven, the substrates were subjected to ultraviolet-ozone for 20 min prior to use. To form the HTL, pristine NiO_x was spin-coated onto the substrates at 4000 rpm for 90 s. The samples were then pre-baked at 150 °C for 5 min and annealed at 300 °C for 1 h to obtain the NiO_x-based HTLs. All perovskite films were coated onto the NiO_x HTLs in a N_2-filled glove box by the process described above. Subsequently, the PCBM (20 mg mL^{-1} in CBZ) ETL was spin-coated onto the perovskite at 3000 rpm for 35 s. Finally, a silver electrode was thermally evaporated under high vacuum ($< 1 \times 10^{-6}$ Torr) after defining an effective cell area of 4 mm^2 with a shadow mask.

2.3. Characterization

The crystalline structures of the perovskite films were characterized by X-ray diffraction (XRD; New D8-Advance, Bruker-AXS). The surface morphologies of the films were observed by field emission scanning electron microscopy (FE-SEM; SIGMA, Carl Zeiss) and atomic force microscopy (AFM; XE-100, Park Systems). The cross sections of the prepared films were also investigated by FE-SEM (SIGMA, Carl Zeiss). The absorption spectra of the films were characterized by ultraviolet–visible (UV–Vis) spectroscopy (UV-2700, Shimadzu). Steady-state PL measurements of the fabricated perovskite films were conducted using a spectrofluorometer (FP-8600, Jasco) with a laser excitation wavelength of 405 nm. For device characterization, all current-voltage (*J-V*) curves of the fabricated PVSCs were characterized using a solar simulator (PEC-L01, Peccell Technologies) under the AM 1.5 standard spectrum (100 mW cm^{-2}) at 25 °C.

3. Result and discussion

Until now, the perovskite absorber layer in most PVSCs has been fabricated through an anti-solvent washing process. However, this process has a critical limitation in terms of large-scale commercialization. Unfortunately, without anti-solvent washing, the surface coverage of the perovskite layer is very difficult to control, and shunting often occurs, resulting in very poor photovoltaic properties when applied to solar cells. Therefore, we aimed to develop a process that does not use anti-solvent washing—instead using PEO, an ionic insulating polymer that has not been applied to the materials of PVSCs. Subsequently, we evaluated the properties of the proposed PEO-perovskite according to the various amounts of PEO added.

Fig. 1 (a) and (b) show the surface and cross-sectional FE-SEM images, respectively, of the $MAPbI_3$ perovskite film made without anti-solvent washing. This film exhibits many large vacancies and pinholes on the surface—which is not uniform. Large voids are also observed in the cross-section. These results are consistent with those previously reported [29–31]. Such vacancies can give rise to serious recombination losses, allowing for direct contact between the ETL and HTL of the upper and lower layers. In comparison, Fig. 1 (c) shows the surface morphology of the $MAPbI_3$ film prepared using the anti-solvent

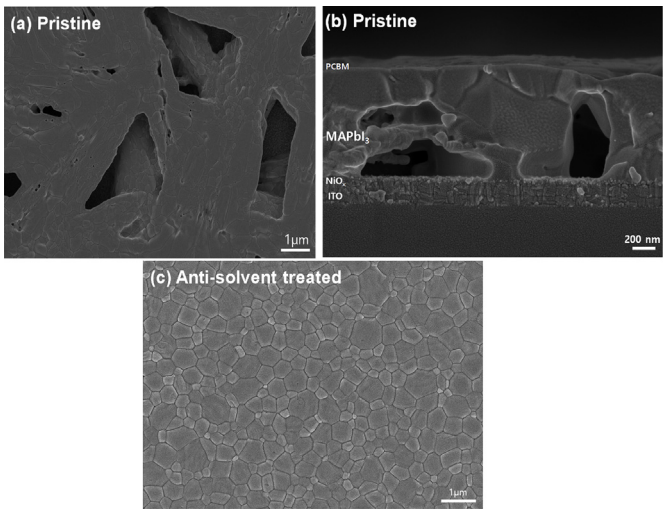

Fig. 1. (a,b) Surface morphology and cross-sectional image of pristine $MAPbI_3$ perovskite film made without anti-solvent washing, and (c) surface morphology of $MAPbI_3$ perovskite film processed with anti-solvent washing.

(chlorobenzene) washing process, in which a very compact surface with no pinholes or vacancies is observed. On this basis, the washing process has been applied to most PVSCs in lab-scale studies to completely solve the morphological problem of unwashed perovskites. However, as mentioned above, it can be expected that commercialization will accelerate if this process—and the associated development of large-scale equipment and difficulty of choosing an environmentally-benign anti-solvent—can be avoided.

To solve these problems, we propose a method of creating an absorber layer by adding PEO—an insulating polymer material—to a conventional $MAPbI_3$ perovskite solution. The process of producing the PEO-perovskite composite thin films is shown in Fig. 2 (a). Fig. 2(b–d) show the surface topographies obtained by FE-SEM. The images illustrate the effect of crystallinity on the morphological properties of the PEO-perovskites with different ratios of PEO/perovskite. As the proportion of PEO increased, the surface became more continuous, surface coverage improved, and grain size became smaller (Fig. S1). The grain size of the perovskite without PEO was approximately 350–700 nm while that of the perovskites with ratios of 1:1, 1.25:1, and 1.5:1 was approximately 150–280 nm, 80–150 nm, and 50–70 nm, respectively. Additionally, as the PEO/perovskite ratio increased, pinholes and vacancies were significantly reduced. Fig. 2(e–g) shows the cross-sectional images of the ITO/NiO_x/PEO-perovskite/PCBM structures with various PEO/perovskite ratios. As shown in figure, the perovskite without PEO has many large voids. However, such voids decreased substantially with each PEO/perovskite ratio increment, with the PEO-perovskite with a ratio of 1.5:1 (Fig. 2 (g)) exhibiting dense and void-free surface coverage. This uniform and compact perovskite absorber layer can suppress undesirable local shunting by preventing direct contact between the HTL and ETL above caused by vacancies, and thereby improve the photovoltaic properties.

It has been demonstrated that the surface structure can be successfully obtained without the washing process by controlling the components of the composite material. Now, we assess this composite material by a structural point of view. The fabricated PEO-perovskite films with various PEO/perovskite ratios (0:1, 1:1, 1.25:1, 1.5:1) were characterized by XRD, as shown in Fig. 3. The major (110) and (220) peaks in the tetragonal crystalline perovskite phase appeared in the perovskite thin film without PEO. The peaks of the PEO-perovskite (1:1, 1.25:1, 1.5:1) films were also characterized by same peaks. However, the XRD spectra of the neat perovskite also showed a PbI_2 peak (12.7°). It is presumed that this peak was observed because the thin film was too nonuniform and roughly formed, such that it did not form a proper $MAPbI_3$ perovskite crystal and residual PbI_2 remained [32]. As the amount of PEO increased, the diffraction intensity tended to decrease compared with that of the sample without PEO. This result indicates that the PEO incorporation reduces the crystallinity of $MAPbI_3$ perovskites, which is also related with reducing the partial concentration of $MAPbI_3$ as PEO is added. To compare more accurately, the Scherrer formula was introduced as follows [33]:

$$\tau = \frac{K\lambda}{\beta cos\theta} \quad (1)$$

where λ is the wavelength (Å) of the Cu-Kα line (1.54 Å), K is the shape factor (generally 0.9), β is the full width at half maximum (FWHM) of the peak (°), θ is the Bragg angle (°), and τ is crystallite size (Å). In the main peak of (110), the crystallite sizes of the PEO-perovskite films according to PEO amount are shown in Table S1. As a result of the calculation, it was evident that the crystallite sizes were reduced to 95.2 nm, 71 nm, 54.7 nm, and 52.9 nm corresponding to PEO/perovskite ratios of 0:1, 1:1, 1.25:1, and 1.5:1, respectively. This result agreed well with the SEM images in Fig. 2, and confirmed that we were successfully able control the crystallinity of the PEO-perovskites (1:1–1.5:1). Additionally, when PEO was added, no meaningful diffraction peaks were observed except for the principal perovskite peaks, and there was no change in the crystalline characteristics.

We then examined the surface topography of the perovskite films by AFM, as shown in Fig. 4. Similar to the SEM images in Fig. 2, the topographical images in Fig. 4 show fewer pinholes and a more compact surface as the PEO/perovskite ratio increased. Additionally, the root mean square (RMS) roughness was measured to be 146.9 nm, 30.9 nm, 21.4 nm, and 19.8 nm corresponding to PEO/perovskite ratios of 0:1, 1:1, 1.25:1, and 1.5:1, respectively. The roughness decreased significantly and more uniform morphologies were obtained as the ratio of PEO/perovskite increased—these phenomena agree with the surface morphologies observed by FE-SEM (Fig. 2). Such roughness reductions can further prevent shunting between ETL and HTL via PEO-perovskites.

Fig. 5 (a) shows an inverted planar device architecture fabricated by a solution process to demonstrate the device effect of the proposed PEO-perovskite. We applied NiO_x for the HTL and $PC_{61}BM$ for the ETL as charge transport layers. Hence, we could make a more meaningful comparison of the PEO-perovskite device characteristics. Fig. 5 (b) shows the *J-V* curves of the PEO-perovskites and that of the perovskite without PEO; the PV parameter variations are detailed in Table 1. All properties of the PVSCs without PEO deteriorated, while the overall

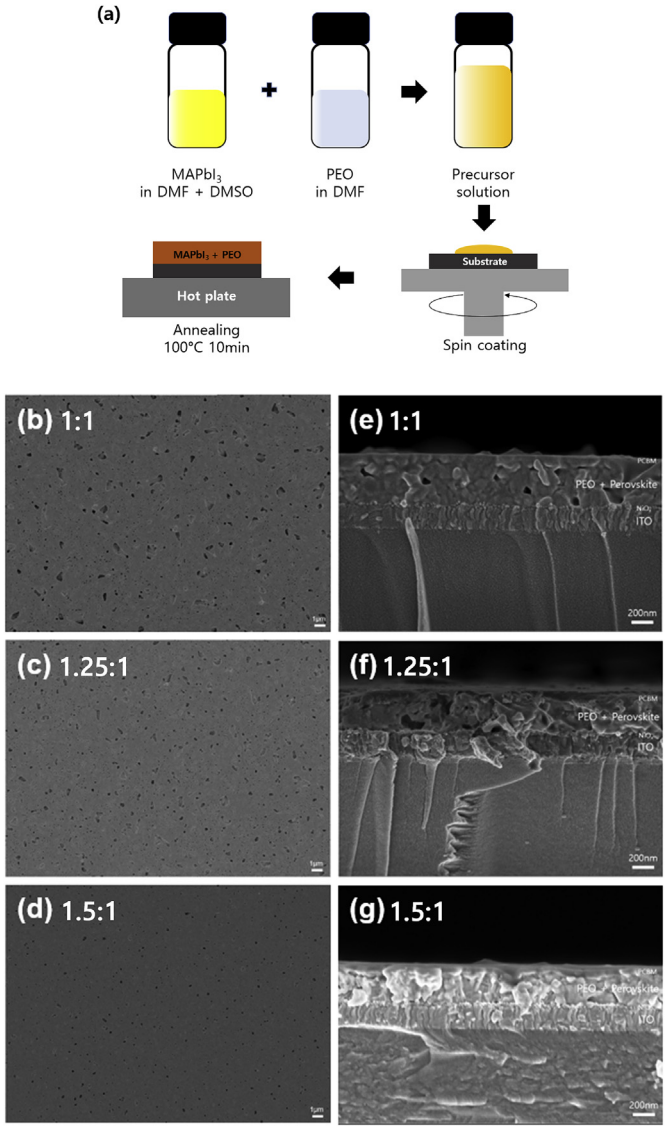

Fig. 2. (a) Processing schematic for PEO-perovskite composite thin films prepared by spin-coating and thermal annealing. FE-SEM images showing the (b,c,d) surface morphologies and (e,f,g) cross-sections of the PEO-perovskite films with PEO/perovskite ratios of (b,e) 1:1, (c,f) 1.25:1, and (d,g) 1.5:1.

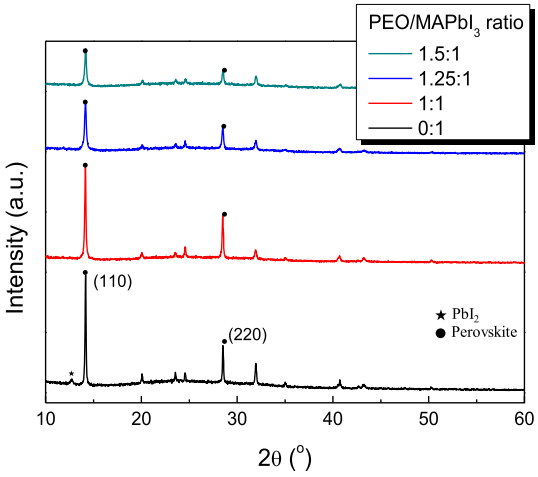

Fig. 3. XRD spectra of PEO-perovskites with various PEO/perovskite ratios.

performance of the PEO-PVSCs was enhanced. As the PEO/perovskite ratio increased (Fig. S2), the Voc and Jsc increased, and the hysteresis index (HI) decreased remarkably from 36% to 11%. These results are in agreement with the SEM images (Fig. 2) and AFM measurements (Fig. 4) and correspond to the alleviation of recombination (caused by pinholes and voids). Fig. 5 (c) and (d) show the *J-V* curves measured to analyze the uniformity and photovoltaic properties of the 9 cells highlighted by the red line Fig. 5 (c; inset). The average photovoltaic parameters of these devices are shown in Table 2. There was only a difference of approximately 8.7% between the best and average efficiencies of the PEO-PVSCs, whereas a large difference of approximately 62% was observed between those of the cells without PEO. Furthermore, solar cells with a larger size (9 mm^2) were measured as shown in Fig. S3. In this case, the overall photovoltaic characteristics of the cell without PEO significantly degraded by 84%, while those of the PEO-perovskite cells only dropped by approximately 25% shown in Table S2. Consequently, we confirmed that the addition of PEO improves the uniformity—even in terms of photovoltaic characteristics. In addition to these properties, we also find the PCE distribution in order to provide the statistical evaluation of the perovskite solar cells, as indicated in Fig. S4. With PEO introduction, we could find better PCE including reproducibility.

Furthermore, we also tried to made PEO-perovskite composition of 2:1 to introduce more PEO in the composite (more than 1.5:1). However, we found that insulating properties in the composite was much pronounced, so it might cause performance degradation of solar cells. We added the device results using PEO-perovskite composition of 2:1, as shown in Fig. S5.

As it is very important to understand the optical and photophysical properties of PEO-perovskite films for the highly improved performance of PEO-PVSCs, we investigated the absorbance and PL properties of the PEO-perovskite films. Fig. 6 (a) shows the absorption spectra for each of the perovskite films. The absorbance of the film without PEO was very low in the short wavelength region, while that of the PEO-perovskite films increased—similar to results in previous work [34]. The poor surface morphology and high pinhole density of the former resulted in insufficient absorption—especially at short wavelengths. However, in the case of the PEO-perovskites, they exhibited an adequate absorption spectrum corresponding to an ideal surface topography with fewer pinholes. The relative concentration of $MAPbI_3$ decreased as the amount of PEO increased because PEO represented a partial volume% of the total solution. Thus, the film thicknesses corresponding to PEO/perovskite ratios of 0:1, 1:1, 1.25:1, and 1.5:1 were 900 nm, 410 nm, 340 nm, and 310 nm, respectively. This thickness variation might also affect the absorption characteristics. Fig. 6 (b) shows the PL intensities of the PEO-perovskite films. The PL intensity of the thin film without PEO was relatively low. In the PEO films, the PL intensity greatly increased with the amount of PEO. This means that when PEO was added to the perovskite, the electronic quality was enhanced—indicated by reduced radiative recombination.

We then focused on the absorbance band edge to analyze the Urbach energy for characterizing the optoelectronic properties of the PEO-perovskite films. As shown in Fig. 6 (c), the band edges of the PEO-perovskite films were sharper than that of the film without PEO. The Urbach energy (E_u), which is the energetic disorder at the band edge, was calculated as a $\alpha = \alpha_0 \exp(E/E_u)$ relation [35], where α is the absorption coefficient (which is extracted from the absorbance spectra), E ($= h\gamma$) is the photon energy, and E_u is the Urbach energy. The resulting

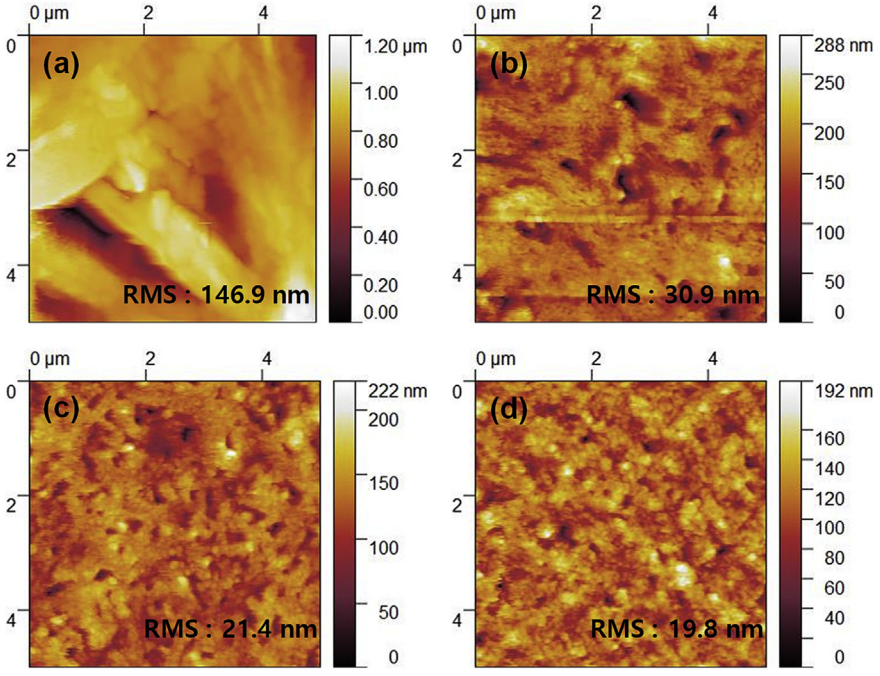

Fig. 4. AFM surface topography images of the films with PEO/perovskite ratios of (a) 0:1, (b) 1:1, (c) 1.25:1, and (d) 1.5:1.

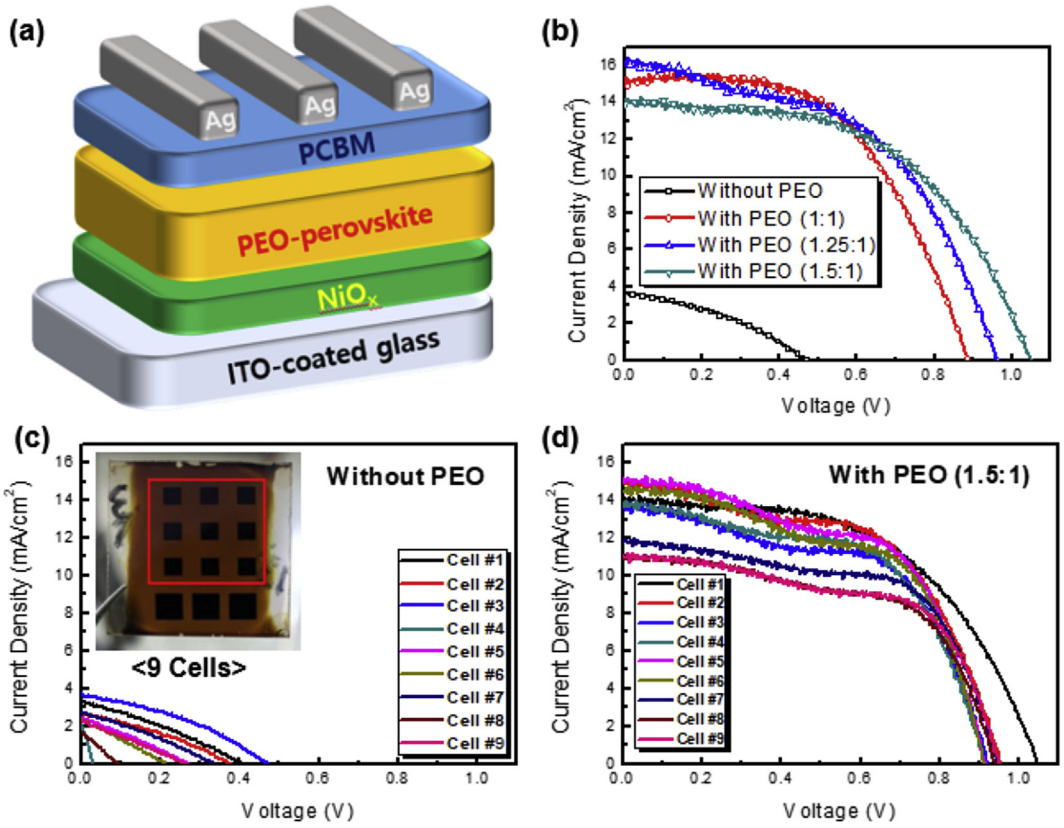

Fig. 5. (a) Device architecture of PEO-PVSCs; (b) *J-V* curves of the best-performing PVSCs without PEO, and those with various PEO/perovskite ratios (1:1–1.5:1); (c) *J-V* curves of the PVSCs (9 cells) without PEO (inset shows a photo of the PEO-perovskite devices on a substrate); (d) those of the PVSCs (9 cells) with PEO (1.5:1).

Table 1
Photovoltaic parameters of the fabricated solar cells under AM 1.5 full illumination.

Cell type	V_{oc} (V)	J_{sc} (mA/cm^2)	FF (%)	PCE(%)
Without PEO	0.47	3.71	36.38	0.63
PEO 1:1	0.89	14.86	57.14	7.52
PEO 1.25:1	0.96	15.97	51.67	7.92
PEO 1.5:1	1.05	13.94	54.39	7.94

E_u values were 61 meV, 55 meV, 41 meV, and 40 meV corresponding to PEO/perovskite ratios of 0:1, 1:1, 1.25:1, and 1.5:1, respectively. The sharper band edges suggest that the PEO additive contributed to a significant reduction in the trap density of the perovskites. These results support those above in that the PEO-perovskites had lower trap-assisted recombination which thereby enhanced the V_{oc} as the amount of PEO increased. These enhancements of the composite material properties could be attributed to the PEO additive in that the PEO chains passivate the grain boundaries and greatly suppress the trap density, thereby remarkably improving the film quality [26].

The initial performance and aging effect (24 h) of the best-performing devices were tested in atmospheric air condition (humidity = 40%); the results are displayed in Fig. S6 and Table S3. The perovskite device without PEO exhibited a large overall reduction in photovoltaic properties of approximately 53%, while the PEO-perovskite device exhibited a very small decrease of approximately 6.5% in PCE. The remarkable stability characteristics of the PEO-PVSCs can be attributed to the suppression of trap-assisted recombination. From these experimental results, the PEO-perovskite composite formation offers promising potential for scalability by eliminating the critical anti-solvent treatment. Though device efficiency presented in this work was rather moderate compared to state-of-the-art PVSCs, we did not apply the critical step of the anti-solvent washing process which promotes the uniform distribution of large crystallites. Additionally, the enhancements of device performance and uniformity, as well as outdoor stability, that were evident in our study can serve as core backgrounds for the rapid industrialization of current PVSC technology.

4. Conclusions

We proposed and fabricated PEO-perovskite composites to avoid the anti-solvent washing process—typically used during perovskite spin coating—and maintained adequate control of the surface topography. Crystallographic, morphological, and optical properties were analyzed according to the various PEO/perovskite ratios. We confirmed a decrease in crystallinity and observed a denser surface, void-free cross section, and fewer pinholes or vacancies as PEO was added. Additionally, AFM analyses demonstrated morphological controllability in that the roughness was significantly reduced by the addition of PEO, despite the lack of an anti-solvent washing process. As a result of

Table 2
Average photovoltaic parameters of 9 PVSCs, and those of 9 PEO-PVSCs.

Cell type	V_{oc} (V)	J_{sc} (mA/cm^2)	FF (%)	PCE(%)
Without PEO (Average of 9 cells)	0.27	2.56	29.80	0.24 (−62%)
PEO 1.5:1 (Average of 9 cells)	0.94	13.28	58.24	7.25 (−8.7%)

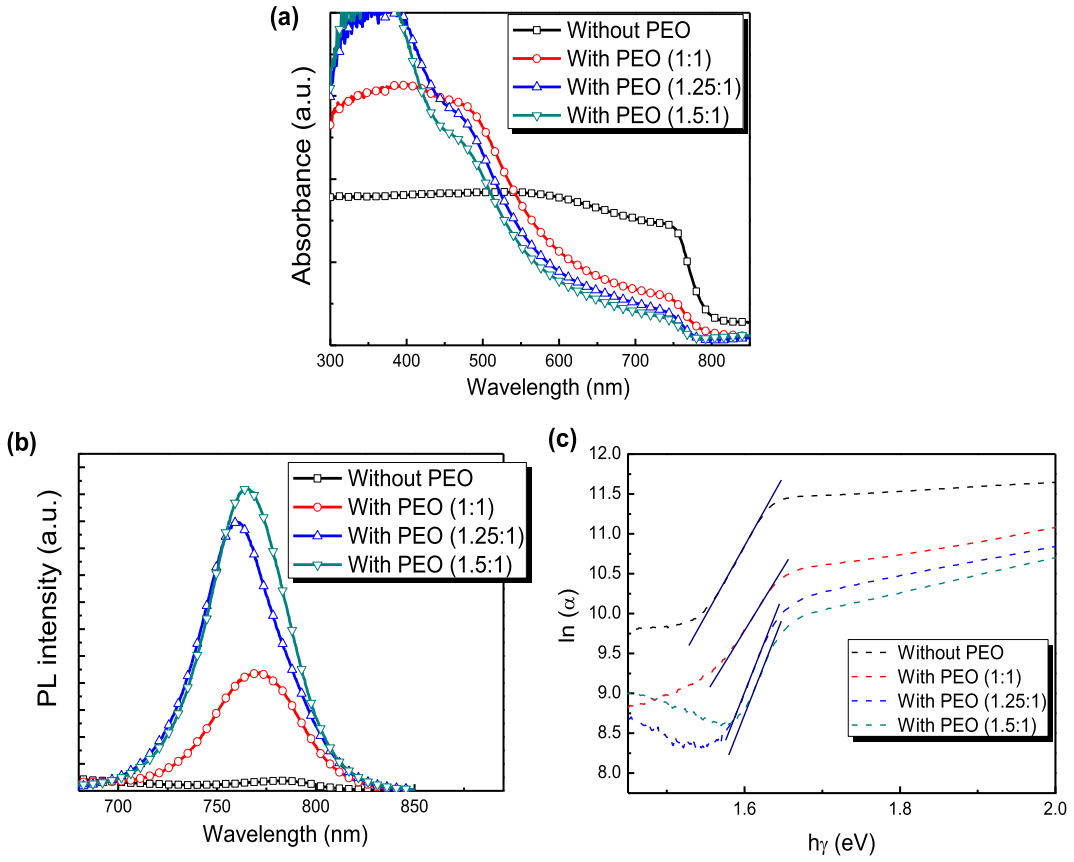

Fig. 6. (a) Absorption and (b) steady-state PL spectra of the perovskite films; (c) plot of the absorption coefficient (α) vs. the photon energy (E = $h\gamma$) used to extract the Urbach energy for the perovskite films.

investigating the optical characteristics, the steady-state PL intensity was found to have increased with the PEO/perovskite ratio, while the Urbach energy value decreased. This indicated that the trap-assisted recombination of the pristine $MAPbI_3$ made without the washing process was greatly reduced. As such, the efficiency of the PEO-PVSCs increased because the overall photovoltaic properties and V_{oc} were enhanced enormously from 0.47 V to 1.05 V. Furthermore, the PEO-PVSCs showed very excellent characteristics in terms of stability. When the device was fabricated with a larger area (9 mm^2), the PEO-PVSCs exhibited a much smaller reduction than the PVSC without PEO. Additionally, the best PEO-PVSC device performance was not significantly different from the average performance in terms of photovoltaic uniformity. These impressive results have introduced a new method for the large-scale commercialization of PVSCs while improving the quality of perovskite films.

Conflicts of interest

There are no conflicts of interest to declare.

Acknowledgements

This work was supported by the National Research Foundation of Korea (NRF) grant funded by the Korea government (MSIT) (NRF-2018R1A4A1024691) and also supported by Chung-Ang University Research Grants in 2018.

Appendix A. Supplementary data

Supporting Information including detail analysis on FE-SEM, J-V hysteresis, and outdoor stability is available.

Supplementary data to this article can be found online at https://doi.org/10.1016/j.ceramint.2019.08.042.

References

[1] M.A. Green, Y. Hishikawa, E.D. Dunlop, D.H. Levi, J. Hohl-Ebinger, A.W. Ho-Baillie, Solar cell efficiency tables (version 52), Prog. Photovolt. Res. Appl. 26 (2018) 427–436 https://doi.org/10.1002/pip.3040.

[2] N.J. Jeon, H. Na, E.H. Jung, T.-Y. Yang, Y.G. Lee, G. Kim, H.-W. Shin, S.I. Seok, J. Lee, J. Seo, A fluorene-terminated hole-transporting material for highly efficient and stable perovskite solar cells, Nat. Energy 3 (2018) 682 https://doi.org/10.1038/s41560-018-0200-6.

[3] L. Protesescu, S. Yakunin, M.I. Bodnarchuk, F. Krieg, R. Caputo, C.H. Hendon, R.X. Yang, A. Walsh, M.V. Kovalenko, Nanocrystals of cesium lead halide perovskites (CsPbX3, X = Cl, Br, and I): novel optoelectronic materials showing bright emission with wide color gamut, Nano Lett. 15 (2015) 3692–3696 https://doi.org/10.1021/nl5048779.

[4] M. Saliba, T. Matsui, K. Domanski, J.-Y. Seo, A. Ummadisingu, S.M. Zakeeruddin, J.-P. Correa-Baena, W.R. Tress, A. Abate, A. Hagfeldt, Incorporation of rubidium cations into perovskite solar cells improves photovoltaic performance, Science 354 (2016) 206–209 https://doi.org/10.1126/science.aah5557.

[5] W.S. Yang, B.-W. Park, E.H. Jung, N.J. Jeon, Y.C. Kim, D.U. Lee, S.S. Shin, J. Seo, E.K. Kim, J.H. Noh, Iodide management in formamidinium-lead-halide–based perovskite layers for efficient solar cells, Science 356 (2017) 1376–1379 https://doi.org/10.1126/science.aan2301.

[6] Y. Li, Z. Shi, L. Lei, F. Zhang, Z. Ma, D. Wu, T. Xu, Y. Tian, Y. Zhang, G. Du, C. Shan, X. Li, Highly stable perovskite photodetector based on vapor-processed micrometer-scale CsPbBr3 microplatelets, Chem. Mater. 30 (2018) 6744–6755 https://doi.org/10.1021/acs.chemmater.8b02435.

[7] J.A. Christians, P. Schulz, J.S. Tinkham, T.H. Schloemer, S.P. Harvey, B.J.T. de Villers, A. Sellinger, J.J. Berry, J.M. Luther, Tailored interfaces of unencapsulated perovskite solar cells for > 1,000 hour operational stability, Nat. Energy 3 (2018) 68 https://doi.org/10.1038/s41560-017-0067-y.

[8] H.J. Snaith, Perovskites: the emergence of a new era for low-cost, high-efficiency solar cells, J. Phys. Chem. Lett. 4 (2013) 3623–3630 https://doi.org/10.1021/jz4020162.

[9] C.V. Kumar, G. Sfyri, D. Raptis, E. Stathatos, P. Lianos, Perovskite solar cell with low cost Cu-phthalocyanine as hole transporting material, RSC Adv. 5 (2015) 3786–3791 https://doi.org/10.1039/C4RA14321C.

[10] S. Casaluci, L. Cinà, A. Pockett, P.S. Kubiak, R.G. Niemann, A. Reale, A. Di Carlo, P. Cameron, A simple approach for the fabrication of perovskite solar cells in air, J. Power Sources 297 (2015) 504–510 https://doi.org/10.1016/j.jpowsour.2015.08.010.

[11] H.S. Jung, N.G. Park, Perovskite solar cells: from materials to devices, Small 11 (2015) 10–25 https://doi.org/10.1002/smll.201402767.

[12] F. Zhang, X. Yang, M. Cheng, W. Wang, L. Sun, Boosting the efficiency and the stability of low cost perovskite solar cells by using CuPc nanorods as hole transport material and carbon as counter electrode, Nano Energy 20 (2016) 108–116 https://doi.org/10.1016/j.nanoen.2015.11.034.

[13] N. Ahn, D.-Y. Son, I.-H. Jang, S.M. Kang, M. Choi, N.-G. Park, Highly reproducible perovskite solar cells with average efficiency of 18.3% and best efficiency of 19.7% fabricated via Lewis base adduct of lead (II) iodide, J. Am. Chem. Soc. 137 (2015) 8696–8699 https://doi.org/10.1021/jacs.5b04930.

[14] Y. Wang, J. Wu, P. Zhang, D. Liu, T. Zhang, L. Ji, X. Gu, Z.D. Chen, S. Li, Stitching triple cation perovskite by a mixed anti-solvent process for high performance perovskite solar cells, Nano Energy 39 (2017) 616–625 https://doi.org/10.1016/j.nanoen.2017.07.046.

[15] S. Paek, P. Schouwink, E.N. Athanasopoulou, K. Cho, G. Grancini, Y. Lee, Y. Zhang, F. Stellacci, M.K. Nazeeruddin, P. Gao, From nano-to micrometer scale: the role of antisolvent treatment on high performance perovskite solar cells, Chem. Mater. 29 (2017) 3490–3498 https://doi.org/10.1021/acs.chemmater.6b05353.

[16] P. Wang, X. Zhang, Y. Zhou, Q. Jiang, Q. Ye, Z. Chu, X. Li, X. Yang, Z. Yin, J. You, Solvent-controlled growth of inorganic perovskite films in dry environment for efficient and stable solar cells, Nat. Commun. 9 (2018) 2225 https://doi.org/10.1038/s41467-018-04636-4.

[17] F. Zhang, J. Song, L. Zhang, F. Niu, Y. Hao, P. Zeng, H. Niu, J. Huang, J. Lian, Film-through large perovskite grains formation via a combination of sequential thermal and solvent treatment, J. Mater. Chem. 4 (2016) 8554–8561 https://doi.org/10.1039/C6TA03115C.

[18] D. Prat, J. Hayler, A. Wells, A survey of solvent selection guides, Green Chem. 16 (2014) 4546–4551 https://doi.org/10.1039/C4GC01149J.

[19] T. Bu, L. Wu, X. Liu, X. Yang, P. Zhou, X. Yu, T. Qin, J. Shi, S. Wang, S. Li, Synergic interface optimization with green solvent engineering in mixed perovskite solar cells, Adv. Energy Mater. 7 (2017) 1700576 https://doi.org/10.1002/aenm.201700576.

[20] C. Liu, W. Li, C. Zhang, Y. Ma, J. Fan, Y. Mai, All-Inorganic $CsPbI_2Br$ perovskite solar cells with high efficiency exceeding 13%, J. Am. Chem. Soc. 140 (2018) 3825–3828 https://doi.org/10.1021/jacs.7b13229.

[21] M. Wang, Q. Fu, L. Yan, P. Guo, L. Zhou, G. Wang, Z. Zheng, W. Luo, Improving the performance and reproducibility of inverted planar perovskite solar cells using tetraethyl orthosilicate as the antisolvent, ACS Appl. Mater. Interfaces 11 (2019) 3909–3916 https://doi.org/10.1021/acsami.8b18402.

[22] T.-R. Chou, S.-H. Chen, Y.-T. Chiang, Y.-T. Lin, C.-Y. Chao, Highly conductive PEDOT:PSS films by post-treatment with dimethyl sulfoxide for ITO-free liquid crystal display, J. Mater. Chem. C 3 (2015) 3760–3766 https://doi.org/10.1039/C5TC00276A.

[23] Y. Ling, Y. Tian, X. Wang, J.C. Wang, J.M. Knox, F. Perez-Orive, Y. Du, L. Tan, K. Hanson, B. Ma, Enhanced optical and electrical properties of polymer-assisted all-inorganic perovskites for light-emitting diodes, Adv. Mater. 28 (2016) 8983–8989 https://doi.org/10.1002/adma.201602513.

[24] C. Wu, Y. Zou, T. Wu, M. Ban, V. Pecunia, Y. Han, Q. Liu, T. Song, S. Duhm, B. Sun, Improved performance and stability of all-inorganic perovskite light-emitting diodes by antisolvent vapor treatment, Adv. Funct. Mater. 27 (2017) 1700338 https://doi.org/10.1002/adfm.201700338.

[25] Y. Tian, C. Zhou, M. Worku, X. Wang, Y. Ling, H. Gao, Y. Zhou, Y. Miao, J. Guan, B. Ma, Highly efficient spectrally stable red perovskite light-emitting diodes, Adv. Mater. 30 (2018) 1707093 https://doi.org/10.1002/adma.201707093.

[26] B. Jeong, H. Han, Y.J. Choi, S.H. Cho, E.H. Kim, S.W. Lee, J.S. Kim, C. Park, D. Kim, C. Park, All-Inorganic $CsPbI_3$ perovskite phase-stabilized by poly (ethylene oxide) for red-light-emitting diodes, Adv. Funct. Mater. 28 (2018) 1706401 https://doi.org/10.1002/adfm.201706401.

[27] L. Zhu, J. Shi, S. Lv, Y. Yang, X. Xu, Y. Xu, J. Xiao, H. Wu, Y. Luo, D. Li, Q. Meng, Temperature-assisted controlling morphology and charge transport property for highly efficient perovskite solar cells, Nano Energy 15 (2015) 540–548 https://doi.org/10.1016/j.nanoen.2015.04.039.

[28] M. Kim, S.G. Motti, R. Sorrentino, A. Petrozza, Enhanced solar cell stability by hygroscopic polymer passivation of metal halide perovskite thin film, Energy Environ. Sci. 11 (2018) 2609–2619 https://doi.org/10.1039/C8EE01101J.

[29] A. Dualeh, N. Tétreault, T. Moehl, P. Gao, M.K. Nazeeruddin, M. Grätzel, Effect of annealing temperature on film morphology of organic–inorganic hybrid pervoskite solid-state solar cells, Adv. Funct. Mater. 24 (2014) 3250–3258 https://doi.org/10.1002/adfm.201304022.

[30] J.W. Jung, S.T. Williams, A.K.-Y. Jen, Low-temperature processed high-performance flexible perovskite solar cells via rationally optimized solvent washing treatments, RSC Adv. 4 (2014) 62971–62977 https://doi.org/10.1039/C4RA13212B.

[31] M. Xiao, F. Huang, W. Huang, Y. Dkhissi, Y. Zhu, J. Etheridge, A. Gray-Weale, U. Bach, Y.B. Cheng, L. Spiccia, A fast deposition-crystallization procedure for highly efficient lead iodide perovskite thin-film solar cells, Angew. Chem. Int. Ed. 53 (2014) 9898–9903 https://doi.org/10.1002/anie.201405334.

[32] N. Timasi, S. Tafazoli, E. Nouri, M.-R. Mohammadi, Y. Li, Solvent engineering based on triethylenetetramine (TETA) for perovskite solar cells processed in ambient-air, Photochem. Photobiol. Sci. 18 (2019) 1228–1234 https://doi.org/10.1039/C9PP00071B.

[33] M. Abdullah, K. Khairurrijal, Derivation of Scherrer relation using an approach in basic physics course, J. Nanosains Nanoteknologi 1 (2009) 28–32.

[34] K. Kara, D.A. Kara, C. Kırbıyık, M. Ersoz, O. Usluer, A.L. Briseno, M. Kus, Solvent washing with toluene enhances efficiency and increases reproducibility in perovskite solar cells, RSC Adv. 6 (2016) 26606–26611 https://doi.org/10.1039/C5RA27122C.

[35] A. Rajagopal, P.-W. Liang, C.-C. Chueh, Z. Yang, A.K.-Y. Jen, Defect passivation via a graded fullerene heterojunction in low-bandgap Pb–Sn binary perovskite photovoltaics, ACS Energy Letters 2 (2017) 2531–2539 https://doi.org/10.1021/acsenergylett.7b00847.